SAND2021-10310C

DC Bus Collection of Type-4 Wind Turbine Farms with Phasing Control to Minimize Energy Storage

Wayne W. Weaver[1],David G. Wilson[2], Rush D. Robinett III[1], Joseph Young[3]
[1]Michigan Technological University, Houghton, Michigan, USA,
[2]Sandia National Labs, Albuquerque, New Mexico, USA
[3]OptimoJoe LLC, Houston, Texas USA

***Abstract*—Typical type-4 wind turbines use DC-link inverters to link the electrical machine to the power grid resulting in 2 power converter steps for each turbine of the N turbine farm and will result in $2N$ power converters. This work presents a DC bus collection system for a type-4 wind farm that reduced the overall required number of converters and minimizes the energy storage system (ESS) requirements. This approach requires one conversion step per turbine, one converter for the ESS and a single grid coupling converter, which leads to $N+2$ number of converters for the wind farm and potentially result in significant cost savings. However, one of the trade-offs for a DC collection system is the need for increased energy storage to filter the power variations and improve power quality to the grid. This paper presents a novel approach to an effective DC bus collection system design. The DC collection for the wind farm implements a power *phasing* control method between turbines that filter the variations and improves power quality while minimizing the need for added energy storage system hardware and improved power quality. The *phasing* control takes advantage of a novel power packet network concept with nonlinear power flow control design techniques that guarantees both stable and enhanced dynamic performance. This paper presents the theoretical design of the DC collection and phasing control. To demonstrate the efficacy of this approach detailed numerical simulation examples are presented.**

I. Introduction

A large number of countries are striving to provide a more reduced carbon-based energy mix economy that is sustainable and secure. Both the European Union (EU) and the United States (US) are including large increases in renewable resources to help meet green energy strategies. For example, in the EU the overall goal by 2030 is to be able to share renewable resources in total energy consumption [1]. In the US, the Department of Energy (DOE), Office of Energy Efficiency and Renewable Energy (EERE) mission is to provide a clean energy economy (carbon-neutral) by 2050. Increased investments in research and development (R&D) will bridge this transition with new technologies [2].

In the last decade wind energy has shown a large growth in installed capacity worldwide [1]. With the introduction of large volumes of renewable energy (RE) integration into the electric power grid (EPG) continued challenges need to be addressed in maintaining reliable grid operations and dynamic stability due to variable generation. Variable power flows due to REs increase the need for reactive power, or energy storage system (ESS) capacity due to both decreased conventional generation and non-collocated RE systems (e.g., offshore wind farms) with load centers requiring long-distance transmission infrastructures [1]. Several of the DOE EERE wind energy technologies office R&D goals are to advance technologies for both onshore and offshore wind with effective EPG integration [3].

Near term energy systems are becoming more distributed and decentralized requiring transmission infrastructures for growing bulk power transfer [3]. Innovative approaches will be required to improve power quality, minimize the number of power electronic components, and reduce ESS requirements. Future power scenarios include offshore wind energy as an important generation source [4]. Numerous researchers [4], [5], [6], [7], [8], [9], [10], [11], [12] are exploring a vast array of approaches to help solve these problems. This new technology is less tolerant to voltage quality disturbances [13] and with widespread use of power electronic converters will contribute to the relevance of power quality [5]. It continues to be critically important to assess the inevitable impact that wind farms have on power quality.

This paper presents a novel approach to an effective DC bus collection system design. The DC collection for the wind farm implements a power phasing control method between turbines that filter the variations and improves power quality while reducing the size and amount of ESS hardware. The phasing control takes advantage of a novel power packet network (PPN) concept [14] with nonlinear power flow control design techniques [15] that guarantees both stable and enhanced dynamic performance. In Section II, the system model is defined that captures the critical coupled dynamics of the mechanical-electrical system. The mechanical-electrical wind turbine coupled models concentrate on a Type IV generator system as part of a DC collective. In Section III, the electrical phasing control is developed that utilizes a PPN electric power grid design technique [14]. In Section IV, a numerical simulation example is presented for a wind farm and DC collective topology. Power electronic and ESS component reductions are reviewed with the trade-off discussed for efficient power quality metrics. Key paper conclusions are given in the last Section.

II. System Model

The schematic of the proposed DC collection system is shown in Fig. 1 where N turbines, which include the electrical induction machine and DC/AC converter, are connected to a common DC collection bus. Also connected to the bus is a generic ESS device that regulates the DC voltage, as well as a grid connected DC/AC inverter. For this work only the DC side of the the grid connected DC/AC is considered.

Sandia National Laboratories is a multimission laboratory managed and operated by National Technology & Engineering Solutions of Sandia, LLC, a wholly owned subsidiary of Honeywell International Inc., for the U.S. Department of Energy's National Nuclear Security Administration under contract DE-NA0003525.

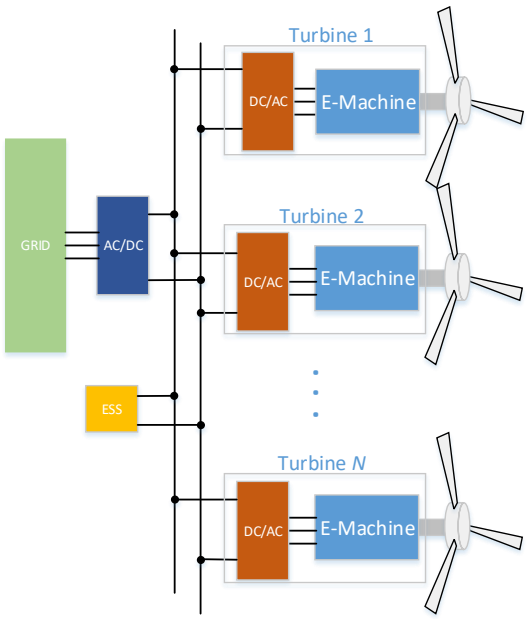

Fig. 1. Wind farm model with ESS.

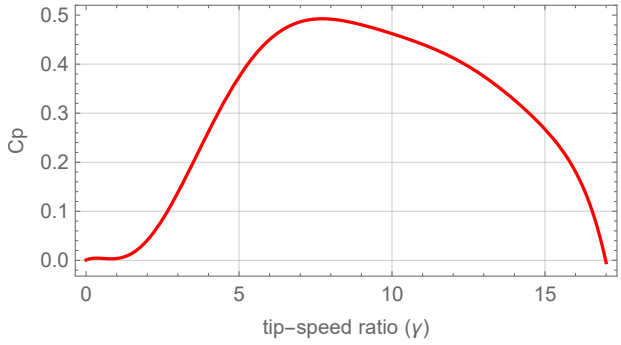

Fig. 2. Power coefficient of Vestas v27 turbine.

The AC dynamics of the grid are not modeled. Further, all power converters are modeled as average-mode behaviour and switching effects are not considered. The following sub-sections will present the models for the individual components including the aerodynamics of the turbine, the electrical induction machine, DC/AC converter, DC bus, ESS and grid connected converter.

A. Turbine and Aerodynamic Model

The aerodynamic power [15] from a each of the wind turbines shown in Fig. 1 is approximated as

$$P_a = \frac{1}{2}\rho\pi R^2 C_p(\gamma)v^3 \tag{1}$$

where ρ is the density of air, R is the rotor radius, v is the wind velocity, and $C_p(\gamma)$ is the power coefficient which is a function of the tip-speed ratio

$$\gamma = \frac{R}{v}\omega_r. \tag{2}$$

The power coefficient curve of the Vestas v27 is shown in Fig. 2.

TABLE I
TURBINE ROTOR MODEL PARAMETERS

Parameter	Description	Value
ρ	Density of air	$1.2kg/m^3$
R	Rotor radius	$13.5\ m$
J	Rotor moment of inertia	$109,900\ kg\ m^2$
B	Friction damping coefficient	$565\ Nm/rad/s$
GR	Gear ratio	38.8
γ_{opt}	Optimal tip-speed ratio for max power	7.7

The aerodynamic torque from the turbine can then be found from

$$\begin{aligned} T_a &= \frac{P_a}{\omega_r} = \frac{1}{2\omega_r}\rho\pi R^2 C_p(\gamma)v^3 \\ &= \frac{1}{2}\rho\pi R^3 C_p(\gamma)v^2. \end{aligned} \tag{3}$$

It should be noted that the pitch of the turbine blades also plays a significant role in the aerodynamic torque T_a and power coefficient C_p. However, in this paper, pitch control is not considered and is left for future study.

Then, the rotational dynamics of the turbine are approximated as

$$J_{turbine}\dot{\omega_r} = T_a - GR\ T_e - \omega_r B \tag{4}$$

where $J_{turbine}$ is the rotational inertia of the rotor, B is the frictional damping, T_e is the electrical torque from the induction machine and GR is the gearbox ratio. The moment of inertia of the turbine is estimated as that of a cylindrical hub with the blades modeled as rods rotating about their ends given as

$$\begin{aligned} J_{turbine} &= J_{hub} + 3J_{blade} \\ &= \left(\frac{1}{2}M_{hub}R_{hub}^2\right) + 3\left(\frac{1}{3}M_{blade}L_{blade}^2\right) \end{aligned} \tag{5}$$

where M_{hub} and R_{hub} are the mass and radius of the hub respectively and M_{blade} and R_{blade} are the mass and radius of the blades. Values for the turbine parameters are taken from the Vestas v27-225 product [16]. TABLE. I contains model parameters values and descriptions of the turbine used in this work.

B. Induction Machine and Inverter Model

A squirrel cage induction machine was chosen as the electrical machine for this work. Further, the specific machine, ABB IDDRPM364004R1 [17] was chosen as the basis of the model and parameters given its power and speed ratings. The differential equating model of the squirrel cage induction machine [18] are

$$\dot{\lambda}_{ds} = v_{ds} - R_s i_{ds} + \omega_s \lambda_{qs} \tag{6}$$

$$\dot{\lambda}_{qs} = v_{qs} - R_s i_{qs} - \omega_s \lambda_{ds} \tag{7}$$

$$\dot{\lambda}_{dr} = 0 - R_r i_{dr} + (\omega_s - p\omega_m)\lambda_{qr} \tag{8}$$

$$\dot{\lambda}_{qr} = 0 - R_r i_{ds} - (\omega_s - p\omega_m)\lambda_{dr} \tag{9}$$

where the state λ_{ds}, λ_{qs}, λ_{dr},λ_{qr} are the flux linkages of the stator d-axes, stator q-axes, rotor d-axes and rotor q-axes respectively. The synchronous speed of the machine is

TABLE II
INDUCTION MACHINE MODEL PARAMETERS

Parameter	Description	Value
R_s	Stator winding resistance	$9.57\ m\Omega$
R_R	Rotor winding resistance	$7.65\ m\Omega$
L_{ls}	Stator leakage inductance	$253\ \mu H$
L_{lr}	Rotor leakage inductance	$253\ \mu H$
L_m	Mutual inductance	$7.07\ mH$
p	Pole-*pairs*	2

ω_s and the mechanical rotor speed is ω_m. The flux linkages can be mapped to the winding currents as

$$\lambda_{ds} = L_{ls} i_{ds} + L_m(i_{ds} + i_{dr}) \tag{10}$$
$$\lambda_{qs} = L_{ls} i_{qs} + L_m(i_{qs} + i_{qr}) \tag{11}$$
$$\lambda_{dr} = L_{lr} i_{dr} + L_m(i_{ds} + i_{dr}) \tag{12}$$
$$\lambda_{qr} = L_{lr} i_{qr} + L_m(i_{qs} + i_{qr}). \tag{13}$$

The electrical torque on the machine shaft is

$$T_e = pL_m(i_{qs} i_{qr} - i_{ds} i_{qr}). \tag{14}$$

Further descriptions and model parameters for this model are given in TABLE. II.

The average-mode reduced order model of the DC/AC inverter is based on [19] and is given as

$$i_{dc} = \alpha(i_{ds}\cos(\delta) + i_{qs}\sin(\delta)) \tag{15}$$
$$v_{ds} = v_{dc}\alpha\cos(\delta) \tag{16}$$
$$v_{qs} = v_{dc}\alpha\sin(\delta) \tag{17}$$

where α is the gain and δ is the phase of the inverter. This model neglects switching effects and gives a simple form for use in the larger system model.

For this application, a *volts-per-hertz* control of the electrical machine [18] was implemented. For the induction machines in this model the optimal ratio is $\beta = 1.22\ V/(rad/s)$. To actuate the torque of the machine a slip control was implemented to control the torque of the electrical machines. In this approach there is a linear approximation between the slip frequency $\omega_{slip} = (\omega_s - p\omega_m)$, and the electrical torque. This linear slip to torque relationship for this model is $k = T_e/\omega_{slip} \approx 315.3\ Nm/(rad/s)$.

C. DC Bus Collection and Energy Storage System Model

Each of the turbines shown in Fig. 1 are connected to a common DC collection bus which has the model

$$\dot{v}_b = \sum_{n=1}^{N} i_{dc,n} - v_b/R_b + u_{ess} - i_{grid} \tag{18}$$

where $i_{dc,n}$ represents the DC currents from the turbine inverters, u_{ess} is the current injected from a generic ESS and i_{grid} is the DC current to a grid connected inverter that serves as the point of common coupling to the larger grid. In this work, the grid dynamics and AC modelling are not considered and i_{grid} set to a fixed value based on the total power generated by the turbines over the time horizon. The energy storage system is modeled as a simple current injection in order to make the ESS device as general and storage-technology agnostic as possible. One of the objectives of this work is to establish a framework that can be used to generate the specifications for the ESS, including peak power, energy capacity. In future work the frequency response and bandwidth of the ESS will be considered as well. Therefore, this model will focus on the energy needs of the system and not the energy capabilities of a specific storage technology such as batteries or super-capacitors [20], [21].

III. ELECTRICAL PHASING CONTROL

To harvest the maximum power from the wind turbine, the wind velocity at the turbine is measured and used to calculate the optimal rotor speed based on the optimal tip-speed ratio $\gamma_{opt} = 7.7$ of the power coefficient from Fig. 2. The optimal aerodynamic torque is then found from (3). Then, assuming the rotor to be in steady-state using (4), the optimal electrical torque T_e is found. The optimal electrical torque from the electrical machine is actuated through the slip control described in Section II-B. A diagram of this process for each individual turbine is shown in Fig. 3.

The ESS injects the required current to keep the bus voltage v_b at a constant $460\ V_{dc}$ in (18). The current to the grid-tie inverter i_{grid} is set to inject the fixed maximum total power collected from the turbines over the period of interest. If the wind values are changing then the sum of powers from the turbines is fluctuating and the ESS must make up the difference to keep v_b constant. However, if the powers injected to the DC bus from the turbines are *phased* over a period then there is less fluctuations in the total.

For this work, a time delay in the wind velocity signal has been introduced into the max power point tracking control shown in Fig. 3. This time delay will cause a sub-optimal power tracking on the turbine, but will also time shift the power injected into the DC bus. When the N turbines in a farm are all equally shifted and spaced over a total delay, then their power fluctuations tend to cancel which causes less effort on the ESS to maintain the bus voltage and thus minimizing the ESS requirements. For example, in a $N = 9$ turbine system with a time delay of $8\ s$, the individual time delays for each of the nine turbines would be $\{0, 1, 2, 3, 4, 5, 6, 7, 8\}\ s$ respectively.

IV. SIMULATION EXAMPLE

To demonstrate the DC collection bus topology with time delay power phasing, a MATLAB/Simulink simulation was constructed from the models described in Section II and the controls described in Section III with nine turbines ($N = 9$). Wind profiles were generated for the system using the NALU wind simulation package [22] for a $600\ s$. The wind profile for each turbine and induction machine are shown in Fig. 4.

A. Baseline Time Delay Example of $0\ s$

To demonstrate a baseline operation, a zero time phase delay was simulated. The resulting rotor speeds in RPM is shown in Fig. 5 and the DC currents from the turbine/induction machines are shown in Fig. 6. Note, the negative sign convention in Fig. 6 denotes currents from the turbines *to* the DC collection bus. The DC collection bus was held at a constant $460\ V_{dc}$ and the current to the grid-connected inverter was $i_{grid} = 3308\ A_{dc}$. The power

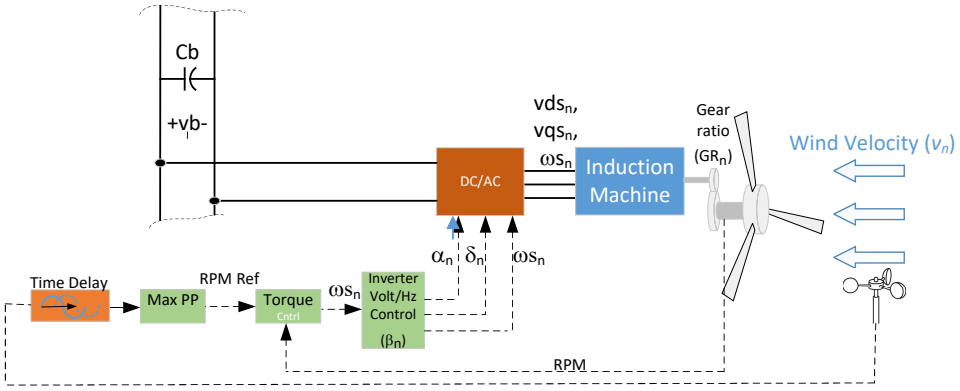

Fig. 3. Turbine control structure.

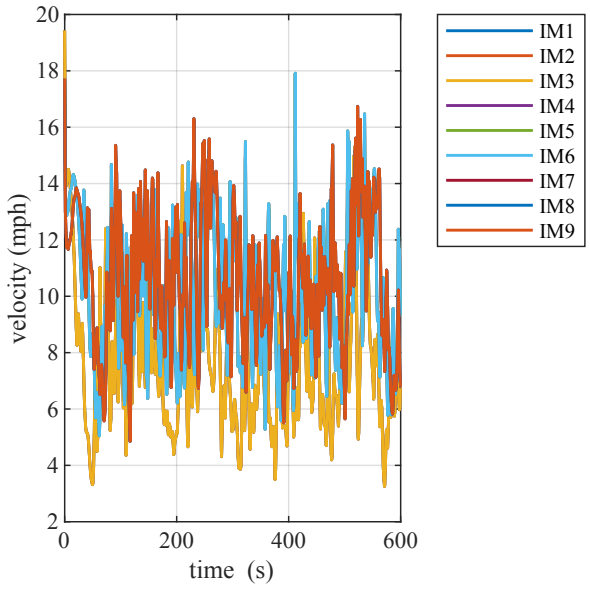

Fig. 4. Wind velocity profiles applied to turbine/induction machine model.

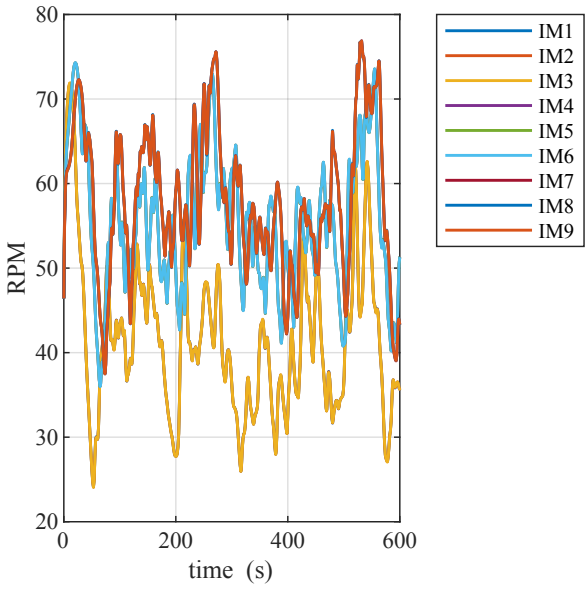

Fig. 5. Rotor RPMs for 0 s phase delay.

and total energy of the ESS are shown in Fig. 7 and Fig. 8, respectively.

B. Time Delay Example of 32 s

To demonstrate the time delay phasing control described in Section III, a total time delay of 32 s was simulated. The resulting rotor speeds in RPM is shown in Fig. 9 and the DC currents from the turbine/induction machines are shown in Fig. 10. The DC collection bus was held at a constant 460 V_{dc} and the current to the grid-connected inverter was $i_{grid} = 3173\ A_{dc}$. The power and total energy of the ESS are shown in Fig. 11 and Fig. 12, respectively.

Note that the DC currents from the turbines in Fig. 10 are more distributed over the 600 s simulation than the baseline case shown in Fig. 6. This enables the ESS to require less effort to maintain the 460 V_{dc} bus and thus use less power and require less energy storage. However, the trade off is that now the power to the grid will be slightly diminished.

C. Overall Results

A batch study was performed using the MATLAB/Simulink model. This study simulated the 600 s period 45 times and increased the phase time delay from 0 s to 90 s in 2 s increments. The resulting peak power of the ESS is shown in Fig. 13, the required energy capacity of the ESS is shown in Fig. 14 and the average grid power is shown in Fig. 15.

It is seen in Fig. 14 that the minimum required energy storage capacity of the ESS is 36.6 MJ and occurs when the phase delay time is 32 s. This is a 18.5% reduction in the capacity over the baseline case of 44.9 MJ. Further, in Fig. 13 it is seen that for a 32 s phase delay time, the peak power is reduced 3% down to 1.81 MW. The cost of implementing the phasing control and reducing the ESS power and energy requirements is that the average power to the grid is also reduced, but only by 3% to 1.46 MW shown in Fig. 15. Therefore, with the DC collection bus and phasing control, significant reductions in the ESS size, weight and likely cost can be made at the expense of a small reduction in total power exported to the grid. Another aspect not quantified in this paper is that power quality to the grid will also be improved with a better regulated DC bus, which occurs with the ESS [23].

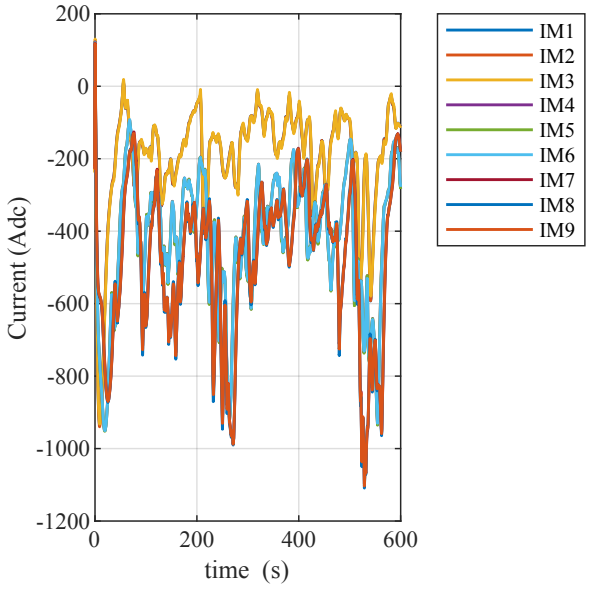

Fig. 6. Turbine DC currents to bus for0 s phase delay.

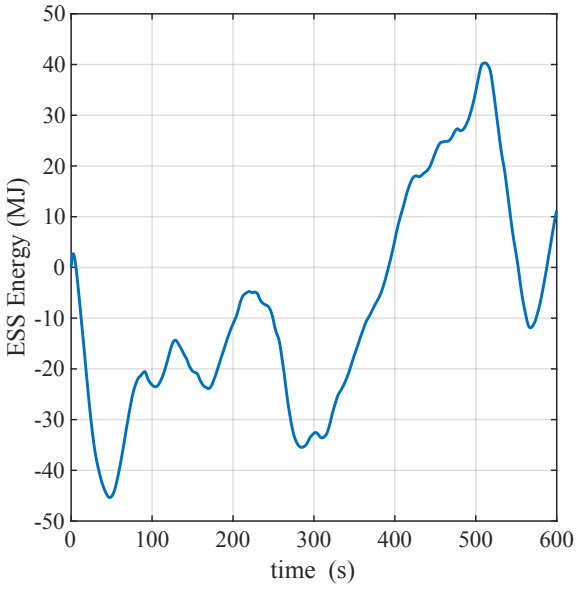

Fig. 8. ESS total stored energy for 0 s phase delay.

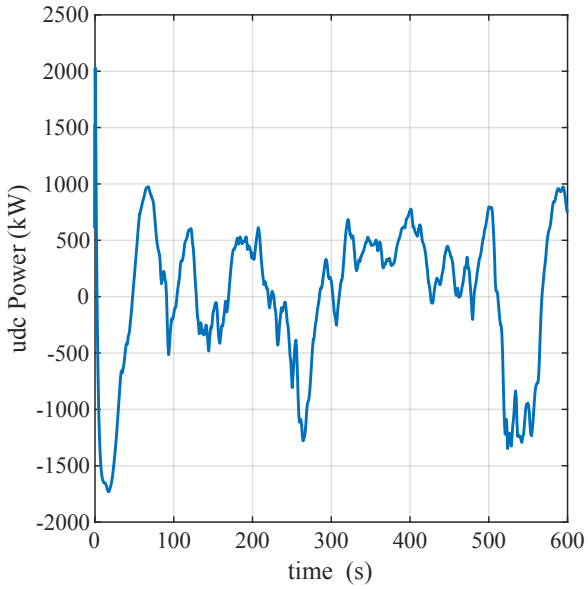

Fig. 7. ESS power for 0 s phase delay.

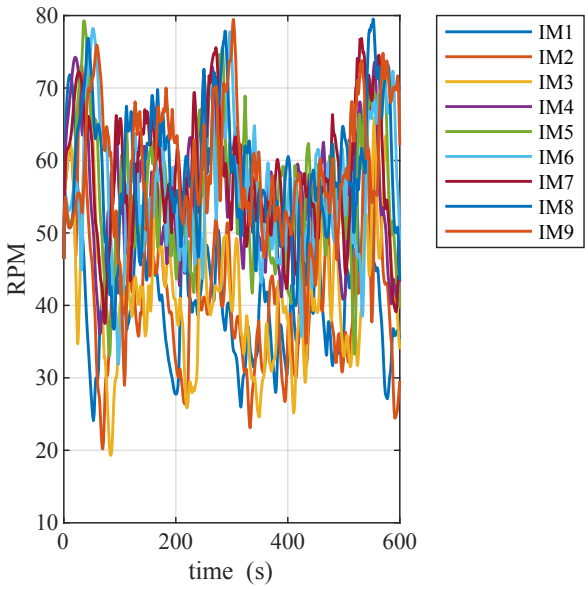

Fig. 9. Rotor RPMs for 32 s phase delay.

V. Conclusion

This work has shown that a DC collection system that utilizes a time delay phasing control of turbines will significantly reduce the ESS requirements. Furthermore, a traditional type-4 wind farm with N turbines will result in $2N$ power converters. The DC collection approach will lead to $N+2$ number of converters, one for each turbine, one for the ESS and one for the grid connected inverter. Further, it is anticipated that incorporation of blade-pitch control of the turbines could also lead to more improvements, but is left for future work. This paper did not quantify the economic impacts, but the reduction in the number of converters, along with the minimization of the ESS and improved power quality to the grid will likely yield a substantial cost savings to the wind farm owner/operator.

VI. Acknowledgments

Sandia National Laboratories is a multimission laboratory managed and operated by National Technology and Engineering Solutions of Sandia, LLC., a wholly owned subsidiary of Honeywell International, Inc., for the U.S. Department of Energy's National Nuclear Security Administration under contract DE-NA0003525. The views expressed in the article do not necessarily represent the views of the U.S. Department of Energy or the United States Government. Special thanks to Dr. Jian Fu at DOE Wind Energy Technology Office for her support for this project. The authors would like to thank, Drs. Alan Hsieh and David Maniaci, Sandia Wind Energy Technologies department for developing the

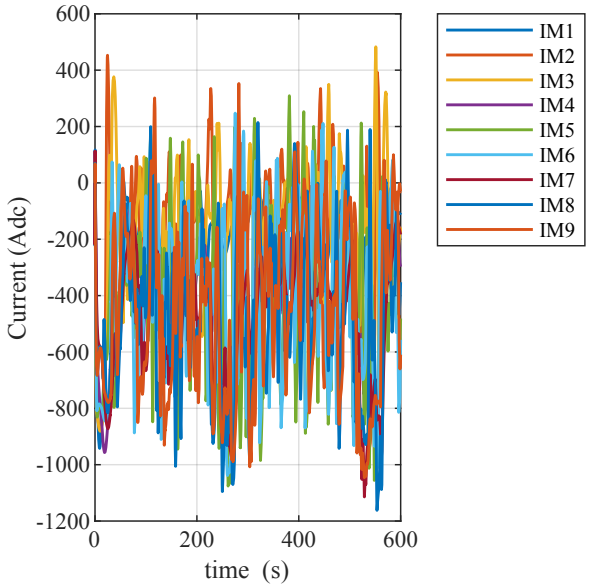

Fig. 10. Turbine DC currents for 32 s phase delay.

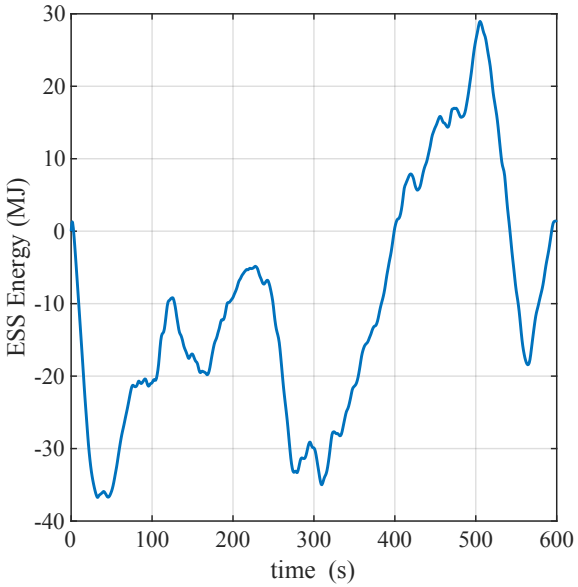

Fig. 12. ESS total energy for 32 s phase delay.

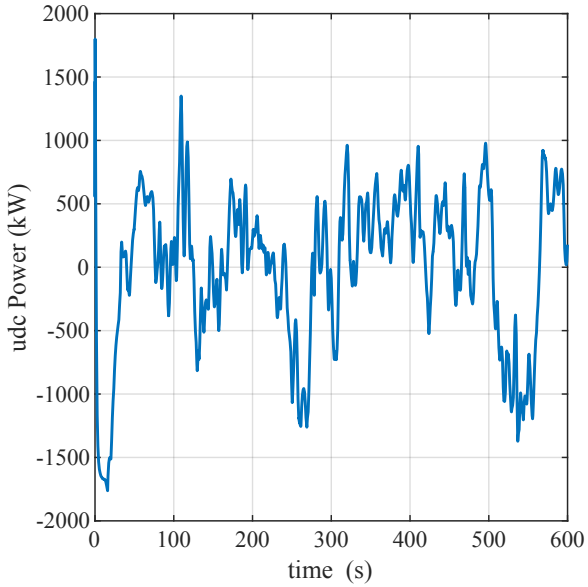

Fig. 11. ESS power for 32 s phase delay.

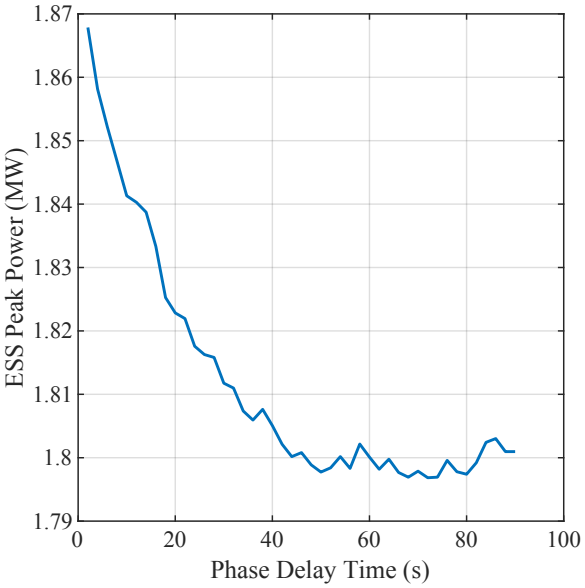

Fig. 13. Peak power of ESS vs turbine phase delay time.

Nalu wind flow fields for the SWiFT facility and providing the corresponding wind profile inputs. This paper approved as SAND2021-XXXXC.

References

[1] A. Jain, J. N. Sakamuri, and N. A. Cutululis, "Grid-forming control strategies for blackstart by offshore wind farms," *Wind Energy Science Discussions*, vol. 2020, pp. 1–22, 2020.

[2] "U.S. department of energy, office of energy efficiency and renewable energy," http://https://www.energy.gov/eere/about-office-energy-efficiency-and-renewable-energy, accessed: 2021-08-19.

[3] "Wind energy technologies office, multi-year program plan, fiscal years 2021-2025," https://www.energy.gov/sites/prod/files/2020/12/f81/weto-multi-year-program-plan-fy21-25-v2.pdf, accessed: 2021-08-19.

[4] A. Fernández-Guillamón, K. Das, N. A. Cutululis, and Á. Molina-García, "Offshore wind power integration into future power systems: Overview and trends," *Journal of Marine Science and Engineering*, vol. 7, no. 11, p. 399, 2019.

[5] F. Blaabjerg and Z. Chen, "Power electronics for modern wind turbines," *Synthesis Lectures on Power Electronics*, vol. 1, no. 1, pp. 1–68, 2005.

[6] J. P. Daniel, S. Liu, E. Ibanez, K. Pennock, G. Reed, and S. Hanes, "National offshore wind energy grid interconnection study," ABB Inc, Tech. Rep., 2014.

[7] M. Fischer, S. Engelken, N. Mihov, and A. Mendonca, "Operational experiences with inertial response provided by type 4 wind turbines," *IET Renewable Power Generation*, vol. 10, no. 1, pp. 17–24, 2016.

[8] D. Nayanasiri and Y. Li, "Formulation of a wind farm control strategy considering lifetime of dc-link capacitor bank of type iv wind turbines," *IET Renewable Power Generation*, 2021.

[9] L. H. Kocewiak, *Harmonics in large offshore wind farms*. Department of Energy Technology, Aalborg University, 2012.

[10] A. Roscoe, P. Brogan, D. Elliott, T. Knueppel, I. Gutierrez, P. Crolla, R. Silva, and J.-C. P. Campion, "Practical experience of providing enhanced grid forming services from an onshore wind park," in *Proc.*

Wind Integration Workshop, 2020.
[11] A. Roscoe, P. Brogan, D. Elliott, T. Knueppel, I. Gutierrez, J. Perez Campion, and R. Da Silva, "Practical experience of operating a grid forming wind park and its response to system events," in *Proceedings Wind Integration Workshop, Dublin, Ireland*, 2019, pp. 16–18.
[12] S. Shah and V. Gevorgian, "Control, operation, and stability characteristics of grid-forming type iii wind turbines," National Renewable Energy Lab.(NREL), Golden, CO (United States), Tech. Rep., 2020.
[13] V. Akhmatov, "Experience with voltage control from large offshore windfarms: the danish case," *Wind Energy: An International Journal for Progress and Applications in Wind Power Conversion Technology*, vol. 12, no. 7, pp. 692–711, 2009.
[14] D. G. Wilson, R. D. Robinett III, W. W. Weaver, M. G. Veurink, and S. F. Glover, "Wec arrays with power packet networks for efficient energy storage and grid integration," in *IEEE/MTS OCEANS*, vol. 1, no. 1, 2021, pp. 1–6.
[15] R. D. Robinett III and D. G. Wilson, *Nonlinear power flow control design: utilizing exergy, entropy, static and dynamic stability, and Lyapunov analysis*. Springer Science & Business Media, 2011.
[16] "Vestas v27-225 general specification," https://backend.orbit.dtu.dk/ws/portalfiles/portal/51244107/ris_m_2861.pdf, accessed: 2021-08-11.
[17] "ABB/Baldor product catalog," https://www.baldor.com/catalog /ID-DRPM364004R1, accessed: 2021-08-11.
[18] P. C. Krause, O. Wasynczuk, S. D. Sudhoff, and S. D. Pekarek, *Analysis of electric machinery and drive systems*. John Wiley & Sons, 2013, vol. 75.
[19] T. Hassell, W. W. Weaver, R. D. Robinett, D. G. Wilson, and G. G. Parker, "Modeling of inverter based ac microgrids for control development," in *IEEE Conference on Control Applications*, vol. 1, no. 1, 2015, pp. 1347–1353.
[20] W. W. Weaver, A. Hagmuller, M. Ginsburg, D. G. Wilson, G. Bacelli, R. D. Robinett, R. Coe, and B. Gunawan, "Wec array networked microgrid control design and energy storage system requirements," in *IEEE OCEANS*. IEEE, 2019, pp. 1–6.
[21] W. W. Weaver, D. G. Wilson, A. Hagmuller, M. Ginsburg, G. Bacelli, R. D. Robinett, R. Coe *et al.*, "Super capacitor energy storage system design for wave energy converter demonstration," in *IEEE International Symposium on Power Electronics, Electrical Drives, Automation and Motion*. IEEE, 2020, pp. 564–570.
[22] M. A. Sprague, S. Ananthan, G. Vijayakumar, and M. Robinson, "Exawind: A multifidelity modeling and simulation environment for wind energy," in *Journal of Physics: Conference Series*, vol. 1452, no. 1. IOP Publishing, 2020, p. 012071.
[23] M. Singh, V. Khadkikar, A. Chandra, and R. K. Varma, "Grid interconnection of renewable energy sources at the distribution level with power-quality improvement features," *IEEE Transactions on Power Delivery*, vol. 26, no. 1, pp. 307–315, 2011.

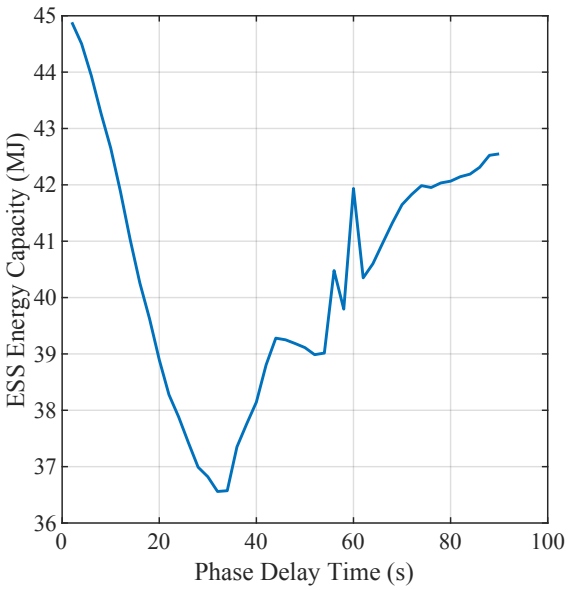

Fig. 14. ESS energy capacity vs turbine phase delay time.

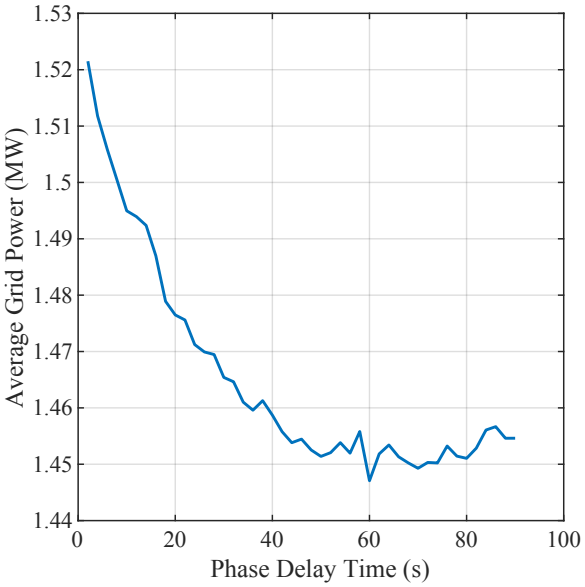

Fig. 15. Average power to the grid vs turbine phase delay time.